

Quantitative analysis of nonadiabatic effects in dense H₃S and PH₃ superconductors

Artur P. Durajski^{1,*}

¹*Institute of Physics, Częstochowa University of Technology,
Ave. Armii Krajowej 19, 42-200 Częstochowa, Poland*

(Dated: July 26, 2021)

The comparison study of high pressure superconducting state of recently synthesized H₃S and PH₃ compounds are conducted within the framework of the strong-coupling theory. By generalization of the standard Eliashberg equations to include the lowest-order vertex correction, we have investigated the influence of the nonadiabatic effects on the Coulomb pseudopotential, electron effective mass, energy gap function and on the $2\Delta(0)/T_C$ ratio. We found that, for a fixed value of critical temperature (178 K for H₃S and 81 K for PH₃), the nonadiabatic corrections reduce the Coulomb pseudopotential for H₃S from 0.204 to 0.185 and for PH₃ from 0.088 to 0.083, however, the electron effective mass and ratio $2\Delta(0)/T_C$ remain unaffected. Independently of the assumed method of analysis, the thermodynamic parameters of superconducting H₃S and PH₃ strongly deviate from the prediction of BCS theory due to the strong-coupling and retardation effects.

Keywords: Superconductivity, hydrogen sulfide, hydrogen phosphide, vertex corrections

PACS numbers: 74.20.Fg, 74.25.Bt, 74.62.Fj

Introduction

The first-principles theoretical studies of the metalization and high-temperature superconductivity of dense hydrogen sulfide were reported for the first time by Li *et al.* in 2014 [1]. This directly initiated the experimental work of Drozdov *et al.* who found that H₂S compressed in a diamond anvil cell exhibit the superconductivity ranging from 30 to 150 K measured in the low-temperature runs [2, 3], which is consistent with calculations mentioned [1]. Furthermore, the results achieved in samples prepared at high-temperature showed that the record critical temperature of 164 K for cooper-oxide system HgBa₂Ca₂Cu₃O_{8+ δ} under quasihydrostatic pressure [4] has been trumped. Based on a sharp drop of the resistivity to zero and an expulsion of the magnetic field, Drozdov *et al.* observed a transition from metal to superconducting state at 203 K in H₂S sample compressed up to 155 GPa [2, 5]. Subsequent theoretical [6–8] and experimental [9, 10] studies suggested that at high pressure, the phase diagram favors decomposition of H₂S into H₃S and elemental sulfur. This result means that the superconducting state observed at 203 K comes from a decomposition product H₃S. More recently, referring to the theoretical crystal structure searches performed by Duan *et al.* [11], the stability of high-pressure cubic $Im\bar{3}m$ structure of H₃S was confirmed by Li *et al.* in first-principles DFT structure searches joined with high-pressure X-ray diffraction experiments [9], and then by Einaga *et al.* in synchrotron X-ray diffraction measurements combined with the electrical resistance measure-

ments [10]. In contrast to cuprates where the nature of superconductivity is still not fully understood [12–14], the presence of a strong isotope effect in H₃S clearly suggests the electron–phonon origin of the superconducting state [2, 15–17]. In addition, Jarlborg and Bianconi predict that the Fermi surface of H₃S consists of multiple sheets similar to those in MgB₂ [18]. However, the existence of multi-gap superconductivity in H₃S has not been so far confirmed.

The above theoretical and experimental discovery have stimulated significant interest in finding new hydrogen-containing superconductors [19–21]. Very recently, Drozdov *et al.* reported superconductivity in compressed PH₃ with a T_C above 100 K [22]. The pressure dependence of the experimental critical temperature for H₃S and PH₃ compounds together with the relevant crystal structures is presented in Fig. 1. For H₃S the second-order structural phase transition from trigonal $R\bar{3}m$ to cubic $Im\bar{3}m$ is experimentally observed at pressure close to 150 GPa [10, 23]. However, according to the static lattice calculations the phase transition from $R\bar{3}m$ to $Im\bar{3}m$ occurs at ~ 180 GPa [11]. A recent theoretical study found that quantum nuclear motion lowers the transition pressure to 103 GPa [24]. In the case of PH₃, a theoretical search of crystal structure reveals two phases with lowest energy: orthorhombic $P2_12_12_1$ and monoclinic $C2/m$. The DFT studies realized by Liu *et al.* indicate that both structures are dynamically stable and superconducting but $C2/m$ phase are in a better agreement with an experimental results [25]. Unfortunately, the lack of structural informations on the superconducting phases from suitable measurements do not allow at this moment for the unambiguous verification of these assumptions.

Motivated by a recent significant experimental and theoretical progress in chemistry and physics of hydrogen-

*Electronic address: adurajski@wip.pcz.pl

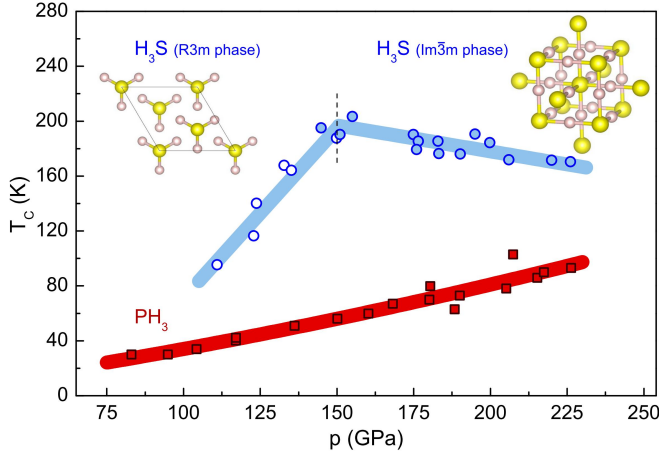


FIG. 1: The experimental data of critical temperature as a function of pressure for H₃S [2, 10] and PH₃ [22]. In addition the stable structures of H₃S [11] are presented.

dense materials, we have carried out calculations to explore in detail the thermodynamic properties of superconducting hydrogen sulfide H₃S and hydrogen phosphide PH₃ at extremely high pressure ($p = 200$ GPa). The very large values of electron-phonon coupling interaction observed in these systems, caused that our investigations were performed within the framework of the Migdal-Eliashberg (ME) theory of superconductivity [26], which goes beyond the BCS model [27] by taking into account the retardation and strong-coupling effects.

This paper is organized as follows. In Section II, we introduce the theoretical model used to determine the quantities characterizing the superconducting state. Moreover, we present details of the first-principles calculations carried out to study the phonon properties and electron-phonon interactions. Then, in Section III, we report and compare the thermodynamic properties of superconducting H₃S and PH₃ systems at 200 GPa. We discuss the validity of the conventional Migdal-Eliashberg theory by introduce the lowest-order vertex correction and we examine its effect on Coulomb pseudopotential, energy gap, $2\Delta(0)/T_C$ ratio and electron effective mass. Finally, we give a summary of this study in Section IV.

Theoretical model and computational methods

Besides the experimental works, most of the theoretical studies concluded that compressed H₃S and PH₃ are phonon-mediated strong-coupling superconductors [8, 11, 25, 28, 29]. Thus, the superconducting state of these compounds can be accurately described by the Migdal-Eliashberg theory [30, 31]. The Eliashberg equations for the superconducting order parameter function $\varphi_n \equiv \varphi(i\omega_n)$ and the electron mass renormalization function $Z_n \equiv Z(i\omega_n)$ written in the imaginary-axis formulation are given by [26, 32]:

$$\varphi_n = \frac{\pi}{\beta} \sum_{m=-M}^M \frac{\lambda_{n,m} - \mu^* \theta(\omega_c - |\omega_m|)}{\sqrt{\omega_m^2 Z_m^2 + \varphi_m^2}} \varphi_m, \quad (1)$$

and

$$Z_n = 1 + \frac{1}{\omega_n} \frac{\pi}{\beta} \sum_{m=-M}^M \frac{\lambda_{n,m}}{\sqrt{\omega_m^2 Z_m^2 + \varphi_m^2}} \omega_m Z_m, \quad (2)$$

where the pairing kernel for the electron-phonon interaction is given by:

$$\lambda_{n,m} = 2 \int_0^{\omega_D} d\omega \frac{\omega}{(\omega_n - \omega_m)^2 + \omega^2} \alpha^2 F(\omega). \quad (3)$$

Moreover, $\beta = 1/k_B T$ and $k_B = 0.0862$ meV/K states the Boltzmann constant. Symbols μ^* and θ denote the screened Coulomb repulsion and the Heaviside function with cut-off frequency ω_c equal to ten times the maximum phonon frequency: $\omega_c = 10\omega_D$.

The application of the above Eliashberg equations to describe the electron-phonon superconductivity is justified for systems in which the value of the phonon energy scale (Debye frequency, ω_D) to the electron energy scale (Fermi energy, ε_F) ratio is negligible. Otherwise the Eliashberg equations should be generalized by taking into account the lowest-order vertex correction [33–37]:

$$\begin{aligned} \varphi_n = & \pi T \sum_{m=-M}^M \frac{\lambda_{n,m} - \mu^* \theta(\omega_c - |\omega_m|)}{\sqrt{\omega_m^2 Z_m^2 + \varphi_m^2}} \varphi_m \\ & - \frac{\pi^3 T^2}{4\varepsilon_F} \sum_{m=-M}^M \sum_{m'=-M}^M \frac{\lambda_{n,m} \lambda_{n,m'}}{\sqrt{(\omega_m^2 Z_m^2 + \varphi_m^2)(\omega_{m'}^2 Z_{m'}^2 + \varphi_{m'}^2)(\omega_{-n+m+m'}^2 Z_{-n+m+m'}^2 + \varphi_{-n+m+m'}^2)}} \\ & \times [\varphi_m \varphi_{m'} \varphi_{-n+m+m'} + 2\varphi_m \omega_{m'} Z_{m'} \omega_{-n+m+m'} Z_{-n+m+m'} - \omega_m Z_m \omega_{m'} Z_{m'} \varphi_{-n+m+m'}], \end{aligned} \quad (4)$$

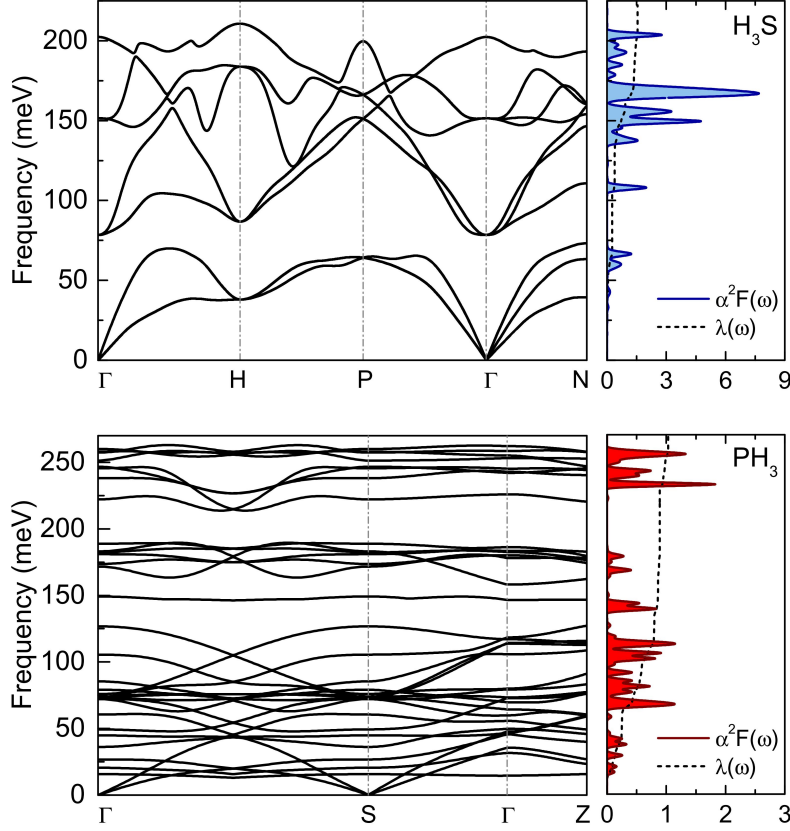


FIG. 2: Phonon dispersion and the Eliashberg spectral function $\alpha^2 F(\omega)$ with electron-phonon integral $\lambda(\omega)$ for H_3S and PH_3 superconductors at 200 GPa.

and

$$\begin{aligned}
 Z_n &= 1 + \frac{\pi T}{\omega_n} \sum_{m=-M}^M \frac{\lambda_{n,m}}{\sqrt{\omega_m^2 Z_m^2 + \varphi_m^2}} \omega_m Z_m \\
 &- \frac{\pi^3 T^2}{4\varepsilon_F \omega_n} \sum_{m=-M}^M \sum_{m'=-M}^M \frac{\lambda_{n,m} \lambda_{n,m'}}{\sqrt{(\omega_m^2 Z_m^2 + \varphi_m^2) (\omega_{m'}^2 Z_{m'}^2 + \varphi_{m'}^2) (\omega_{-n+m+m'}^2 Z_{-n+m+m'}^2 + \varphi_{-n+m+m'}^2)}} \\
 &\times [\omega_m Z_m \omega_{m'} Z_{m'} \omega_{-n+m+m'} Z_{-n+m+m'} + 2\omega_m Z_m \varphi_{m'} \varphi_{-n+m+m'} - \varphi_m \varphi_{m'} \omega_{-n+m+m'} Z_{-n+m+m'}],
 \end{aligned} \tag{5}$$

where, the modified electron-phonon pairing kernel takes the following form:

$$\lambda_{n,m} = 2 \int_0^{\omega_D} d\omega \frac{\omega}{\omega^2 + 4\pi^2 T^2 (\omega_n - \omega_m)^2} \alpha^2 F(\omega). \tag{6}$$

The Eliashberg spectral function, one of the main input element to the Eliashberg equations, is defined as:

$$\alpha^2 F(\omega) = \frac{1}{2\pi N(0)} \sum_{\mathbf{q}\nu} \delta(\omega - \omega_{\mathbf{q}\nu}) \frac{\gamma_{\mathbf{q}\nu}}{\hbar \omega_{\mathbf{q}\nu}} \tag{7}$$

with

$$\begin{aligned}
 \gamma_{\mathbf{q}\nu} &= 2\pi \omega_{\mathbf{q}\nu} \sum_{ij} \int \frac{d^3 k}{\Omega_{BZ}} |g_{\mathbf{q}\nu}(\mathbf{k}, i, j)|^2 \delta(\epsilon_{\mathbf{q},i} - \epsilon_F) \\
 &\times \delta(\epsilon_{\mathbf{k}+\mathbf{q},j} - \epsilon_F),
 \end{aligned} \tag{8}$$

where $N(0)$, $\gamma_{\mathbf{q}\nu}$ and $g_{\mathbf{q}\nu}(\mathbf{k}, i, j)$ denote the density of states at the Fermi energy, the phonon linewidth and the electron-phonon coefficients, respectively. The $\alpha^2F(\omega)$ functions for H_3S and PH_3 were calculated in this paper using density functional perturbation theory and the plane-wave pseudopotential method, as implemented in the Quantum-Espresso package [38]. We assume that H_3S has cubic crystal $Im\bar{3}m$ structure with lattice parameter $a = 2.984 \text{ \AA}$ [11], whereas PH_3 crystallize in monoclinic $C2/m$ structure with lattice parameter $a = 5.152 \text{ \AA}$, $b = 2.961 \text{ \AA}$, $c = 2.960 \text{ \AA}$, $\alpha = \gamma = 90^\circ$ and $\beta = 90.23^\circ$ [39]. The Vanderbilt-type ultrasoft pseudopotentials for S, P and H atoms were employed with a kinetic energy cutoff equal to 80 Ry. The phonon calculations were performed for $32 \times 32 \times 32$ Monkhorst-Pack k -mesh with gaussian smearing of 0.03 Ry. The electron-phonon coupling matrices were computed using $8 \times 8 \times 8$ q -grid for H_3S and $4 \times 4 \times 4$ q -grid for PH_3 . The calculated phonon band structures together with the Eliashberg spectral functions and electron-phonon integrals $\lambda(\omega) = 2 \int_0^{\Omega_{\text{max}}} \omega^{-1} \alpha^2 F(\omega) d\omega$ for both investigated hydrides are presented in Fig. 2. The absence of imaginary frequencies in the full phonon spectra indicates that both systems are dynamically stable.

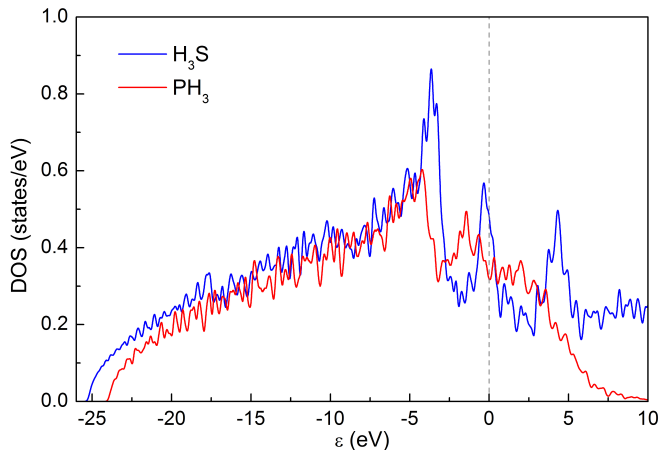


FIG. 3: Density of states (DOS) for H_3S ($Im\bar{3}m$) and PH_3 ($C2/m$) at 200 GPa. The dotted line at zero indicates the Fermi level.

The electronic band structures of H_3S and PH_3 at 200 GPa were also explored. The investigated compounds are good metals with a large density of states (DOS) at the Fermi level. To clarify the difference of the electronic structures between $Im\bar{3}m$ H_3S and $C2/m$ PH_3 , the DOS calculated for these two crystal structures are shown in Fig. 3. A strong peak around the Fermi level (the Van Hove singularities) is favorable for a strong electron-phonon coupling and thus really high superconducting temperature in the case of H_3S [40].

Our *ab-initio* studies showed that ratio $\lambda\omega_D/\varepsilon_F$ is equal to 0.020 for H_3S and 0.014 for PH_3 . These values

are rather small in comparison to fullerene compounds or high- T_c cuprates, however, are not zero. Due to the above, we decided to conduct our calculations simultaneously using the conventional Eliashberg equations and equations with the lowest-order vertex correction, which allows us to examine the influence of nonadiabatic effects on the thermodynamic properties in studied compounds. The numerical analysis was performed using a self-consistent iteration methods [41], which were implemented successfully in our previous papers [31, 42–44]. The convergence and precision of our results are controlled by assuming the sufficiently high number ($M = 1100$) of Matsubara frequencies $\omega_n \equiv (\pi/\beta)(2n - 1)$, where $n = 0, \pm 1, \pm 2, \dots, \pm M$.

Results and discussion

To study the thermodynamic properties of phonon-mediated superconductors on the quantitatively level in the first step we determine the critical value of the Coulomb pseudopotential μ_C^* . For this purpose, in the Eliashberg equations we replace T by the experimental value of critical temperature: $T_C = 178 \text{ K}$ for H_3S [2] and $T_C = 81 \text{ K}$ for PH_3 [22]. Then, starting from zero, we increase the value of μ^* until we reach the equality $\Delta_{m=1}(\mu^* = \mu_C^*) = 0$, where the order parameter is defined as: $\Delta_m = \varphi_m/Z_m$ [45]. The obtained results are presented in Fig. 4. In particular, on the basis of the

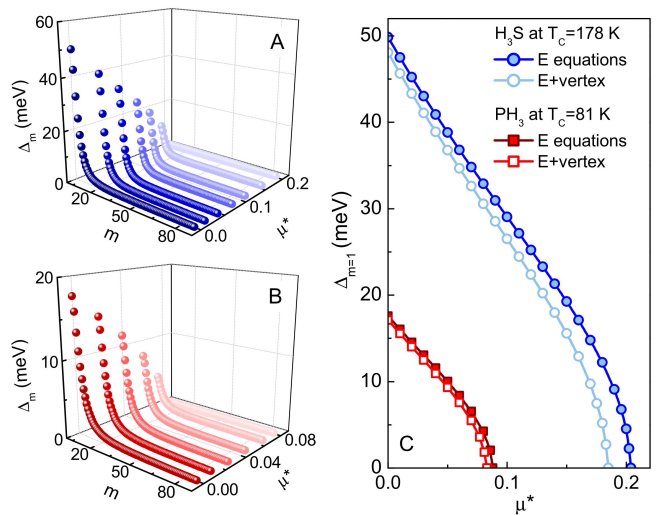


FIG. 4: The order parameter on the imaginary axis as a function of m and μ^* for (A) H_3S and (B) PH_3 at 200 GPa - the results was obtained using conventional Eliashberg (E) equations. (C) The full dependence of the first value of the order parameter as a function of Coulomb pseudopotential.

full dependence of $\Delta_{m=1}(\mu^*)$ we can conclude that if we take into account the conventional Eliashberg equations, the Coulomb pseudopotential takes a relatively high crit-

ical value for H_3S ($\mu_C^* = 0.204$) and low value for PH_3 ($\mu_C^* = 0.088$) at 200 GPa. Moreover, at this point we can found that, for a fixed value of critical temperature, the lowest-order vertex correction changes μ_C^* by -9.3% for H_3S and -5.7% for PH_3 .

In the next step, by using the analytical continuation of the imaginary-axis solutions to the real frequency axis [46], we calculate the temperature dependence of superconducting energy gap $\Delta(T) = \text{Re}[\Delta(\omega = \Delta(T), T)]$ [45]. The obtained results are presented in Fig. 5. Knowledge of the energy gap value at zero temperature

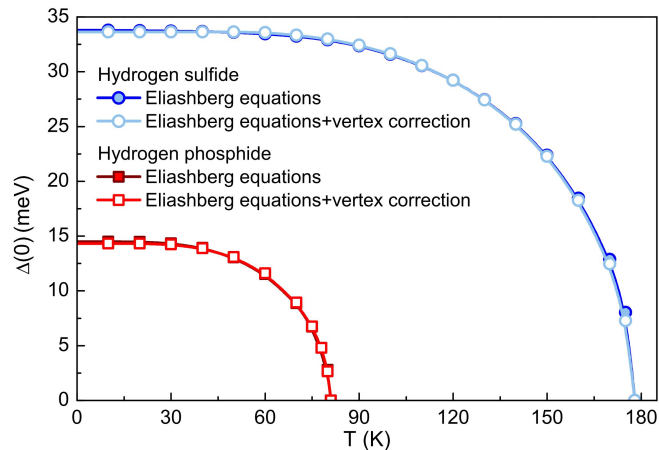


FIG. 5: The temperature dependence of the superconducting energy gap. The numerical results can be reproduced using the analytical formula $\Delta(T) = \Delta(0) \sqrt{1 - (T/T_C)^\alpha}$, where $\alpha = 3.36$.

allowed us to calculate the dimensionless ratio $R_\Delta \equiv 2\Delta(0)/T_C$ for which the BCS theory predicts universal value $[R_\Delta]_{\text{BCS}} = 3.53$. In the case of studied hydrides, R_Δ exceed the value of 4, in particular by using the conventional Eliashberg equations we received $[R_\Delta]_{\text{H}_3\text{S}} = 4.41$ and $[R_\Delta]_{\text{PH}_3} = 4.15$. This behavior is connected with the strong-coupling and retardation effects, which in the framework of the Eliashberg formalism can be characterized by the ratio T_C/ω_{ln} , where ω_{ln} is the logarithmic phonon frequency, correspondingly 131 meV for H_3S and 79 meV for PH_3 . Thus, the considered ratio equals 0.12 and 0.09, respectively, while in the weak-coupling BCS limit we have: $T_C/\omega_{\text{ln}} \rightarrow 0$. Moreover, we find that although the vertex corrections seriously reduce μ_C^* for H_3S and PH_3 , the ratio $2\Delta(0)/T_C$ remains practically unaffected. Similar situation is observed in the case of electron effective mass at T_C calculated from $m_e^* = \text{Re}[Z(0)]m_e$, where m_e denotes the electron band mass. In our case $m_e^*/m_e = 2.736$ for H_3S and $m_e^*/m_e = 2.136$ for PH_3 , regardless of the equations applied. This means that the thermodynamic properties of phonon-mediated superconductors can be successfully obtained in the framework of the conventional Migdal-Eliashberg formalism with the proviso that μ_C^* has to be

accurately determined.

In the last step, to investigate the specific heat and thermodynamic critical field behavior, the condensation energy was numerically calculated:

$$\frac{E_{\text{cond}}(T)}{N(0)} = -\frac{2\pi}{\beta} \sum_{n=1}^M \left(\sqrt{\omega_n^2 + \Delta_n^2} - |\omega_n| \right) \times \left(Z_n^N \frac{|\omega_n|}{\sqrt{\omega_n^2 + \Delta_n^2}} - Z_n^S \right), \quad (9)$$

where Z_n^N and Z_n^S denote the mass renormalization functions for the normal and superconducting states, respectively. The specific heat difference between superconducting and normal state was then obtained from the second derivative of $E_{\text{cond}}(T)$:

$$\frac{\Delta C(T)}{k_B N(0)} = \frac{1}{\beta} \frac{d^2 [E_{\text{cond}}(T)/N(0)]}{d(k_B T)^2} \quad (10)$$

and thermodynamic critical field is defined as:

$$\frac{H_C(T)}{\sqrt{N(0)}} = \sqrt{8\pi [E_{\text{cond}}(T)/N(0)]}. \quad (11)$$

The temperature dependence of ΔC , with characteristic specific heat jump at T_C marked by vertical line, is presented in Fig. 6.

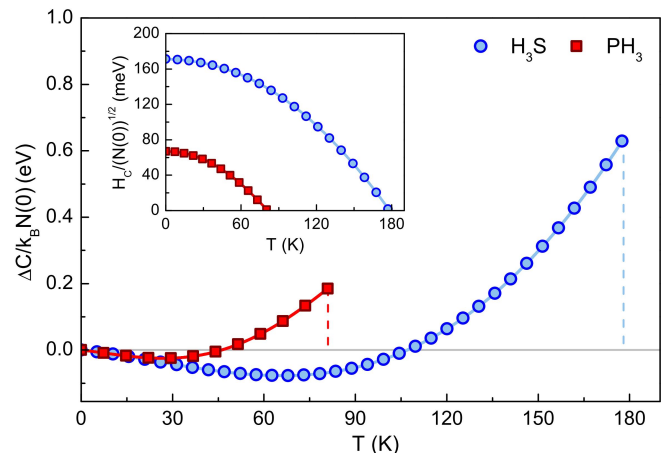


FIG. 6: The specific heat difference between the superconducting and the normal state as a function of temperature. Inset presents the temperature dependence of the thermodynamic critical field.

The inset shows the thermodynamic critical field for investigated hydrides. These results allow us to determine the other two fundamental dimensionless ratios: $R_H \equiv T_C C^N(T_C)/H_C^2(0)$ and $R_C \equiv \Delta C(T_C)/C^N(T_C)$, where the specific heat for the normal state is defined as $C^N = \gamma T$, and γ denotes the Sommerfeld constant: $\gamma \equiv (2/3)\pi^2(1 + \lambda)k_B^2 N(0)$. It is noteworthy that, in the framework of the BCS theory, these ratios adopt universal values of 0.168 and 1.43, respectively [45]. We

emphasize that these dimensionless ratios, similar to that of energy gap, take non-BCS values, in particular: $R_H = 0.136$, $R_C = 2.47$ for H_3S and $R_H = 0.150$, $R_C = 1.99$ for PH_3 . We can see that with increasing values of T_C/ω_{ln} ratio the thermodynamic properties take increasingly non-BCS behavior.

Conclusions

In this work, using the first-principles calculations and Eliashberg theory with and without vertex corrections, we systematically study the nonadiabatic effects on the superconductivity of compressed H_3S and PH_3 compounds. We find that for a fixed experimental value of critical temperature the lowest-order vertex correction reduces the Coulomb pseudopotential (from 0.204 to 0.185 in the case of H_3S and from 0.088 to 0.083 for PH_3), however, the energy gap, electron effective mass and ratio $2\Delta(0)/T_C$ remain unaffected. It means that the superconducting behavior can be properly determined even in the framework of the classical Migdal-Eliashberg formalism, as long as the value of the Coulomb pseudopotential is correctly determined. Moreover, we calculated the specific heat and thermodynamic critical field and we proved that strong-coupling and retardation effects caused that thermodynamic properties of H_3S and PH_3 at high pressures cannot be correctly estimated in the framework of the BCS theory.

Acknowledgements

Author would like to express his gratitude to Krzysztof Durajski, for his assistance in the numerical calculations. Research reported in this paper was financially supported by the Czestochowa University of Technology under Grant No. BS/MN-203-301/2016.

-
- [1] Li, Y., Hao, J., Liu, H., Li, Y. & Ma, Y. The metallization and superconductivity of dense hydrogen sulfide. *J. Chem. Phys.* **140**, 174712 (2014).
- [2] Drozdov, A. P., Eremets, M. I., Troyan, I. A., Ksenofontov, V. & Shylin, S. I. Conventional superconductivity at 203 kelvin at high pressures in the sulfur hydride system. *Nature* **525**, 73 (2015).
- [3] Ma, Y. Near-room-temperature superconductivity in hydrogen sulfide. *NPG Asia Materials* **8**, e236 (2016).
- [4] Gao, L. *et al.* Superconductivity up to 164 K in $HgBa_2Ca_{m-1}Cu_mO_{2m+2+\delta}$ ($m=1, 2$, and 3) under quasi-hydrostatic pressures. *Phys. Rev. B* **50**, 4260–4263 (1994).
- [5] Troyan, I. *et al.* Observation of superconductivity in hydrogen sulfide from nuclear resonant scattering. *Science* **351**, 1303–1306 (2016).
- [6] Bernstein, N., Hellberg, C. S., Johannes, M. D., Mazin, I. I. & Mehl, M. J. What superconducts in sulfur hydrides under pressure and why. *Phys. Rev. B* **91**, 060511 (2015).
- [7] Duan, D. *et al.* Pressure-induced decomposition of solid hydrogen sulfide. *Phys. Rev. B* **91**, 180502 (2015).
- [8] Errea, I. *et al.* High-pressure hydrogen sulfide from first principles: A strongly anharmonic phonon-mediated superconductor. *Phys. Rev. Lett.* **114**, 157004 (2015).
- [9] Li, Y. *et al.* Dissociation products and structures of solid H_2S at strong compression. *Phys. Rev. B* **93**, 020103 (2016).
- [10] Einaga, M. *et al.* Crystal structure of the superconducting phase of sulfur hydride. *Nat. Phys.* **12**, 835–838 (2016).
- [11] Duan, D. *et al.* Pressure-induced metallization of dense $(H_2S)_2H_2$ with high- T_C superconductivity. *Sci. Rep.* **4**, 6968 (2014).
- [12] Zhao, G. The pairing mechanism of high-temperature superconductivity: experimental constraints. *Phys. Scripta* **83**, 038302 (2011).
- [13] Szczęśniak, R. Pairing mechanism for the high- t_c superconductivity: Symmetries and thermodynamic properties. *PLoS ONE* **7**, e31873 (2012).
- [14] Chen, Q. & Wang, J. Pseudogap phenomena in ultracold atomic fermi gases. *Front. Phys.* **9**, 539 – 570 (2014).
- [15] Mazin, I. I. Superconductivity: Extraordinarily conventional. *Nature* **525**, 40–41 (2016).
- [16] Nicol, E. J. & Carbotte, J. P. Comparison of pressurized sulfur hydride with conventional superconductors. *Phys. Rev. B* **91**, 220507 (2015).
- [17] Ortenzi, L., Cappelluti, E. & Pietronero, L. Band structure and electron-phonon coupling in H_3S : A tight-binding model. *Phys. Rev. B* **94**, 064507 (2016).
- [18] Jarlborg, T. & Bianconi, A. Breakdown of the migdal approximation at Lifshitz transitions with giant zero-point motion in h_3s superconductor. *Sci. Rep.* **6**, 24816 (2016).
- [19] Ge, Y., Zhang, F. & Yao, Y. First-principles demonstration of superconductivity at 280 K in hydrogen sulfide with low phosphorus substitution. *Phys. Rev. B* **93**, 224513 (2016).
- [20] Zhong, X. *et al.* Tellurium hydrides at high pressures: High-temperature superconductors. *Phys. Rev. Lett.* **116**, 057002 (2016).
- [21] Zhang, S. *et al.* Tellurium hydrides at high pressures: High-temperature superconductors. *Sci. Rep.* **5**, 15433 (2015).
- [22] Drozdov, A. P., Eremets, M. I. & Troyan, I. A. Superconductivity above 100 K in PH_3 at high pressures. *preprint at arxiv.org/abs/1508.06224* (2015).
- [23] Gor'kov, L. P. & Kresin, V. Z. Pressure and high- t_c superconductivity in sulfur hydrides. *Sci. Rep.* **6**, 25608 (2016).
- [24] Errea, I. *et al.* Quantum hydrogen-bond symmetrization in the superconducting hydrogen sulfide system. *Nature* **532**, 81 (2016).
- [25] Liu, H., Li, Y., Gao, G., Tse, J. S. & Naumov, I. I. Crystal structure and superconductivity of PH_3 at high pressures. *J. Phys. Chem. C* **120**, 3458–3461 (2016).
- [26] Eliashberg, G. M. Interactions between electrons and lattice vibrations in a superconductor. *J. Exp. Theor. Phys.* **11**, 696 (1960).
- [27] Bardeen, J., Cooper, L. N. & Schrieffer, J. R. Theory of superconductivity. *Phys. Rev.* **108**, 1175–1204 (1957).
- [28] Akashi, R., Kawamura, M., Tsuneyuki, S., Nomura,

- Y. & Arita, R. First-principles study of the pressure and crystal-structure dependences of the superconducting transition temperature in compressed sulfur hydrides. *Phys. Rev. B* **91**, 224513 (2015).
- [29] Flores-Livas, J. A. *et al.* Superconductivity in metastable phases of phosphorus-hydride compounds under high pressure. *Phys. Rev. B* **93**, 020508 (2016).
- [30] Durajski, A. P., Szczęśniak, R. & Li, Y. Non-BCS thermodynamic properties of H₂S superconductor. *Physica C* **515**, 1 (2015).
- [31] Durajski, A. P., Szczęśniak, R. & Pietronero, L. High-temperature study of superconducting hydrogen and deuterium sulfide. *Ann. Phys. (Berlin)* **528**, 358–364 (2016).
- [32] Marsiglio, F., Schossmann, M. & Carbotte, J. P. Iterative analytic continuation of the electron self-energy to the real axis. *Physical Review B* **37**, 4965 (1988).
- [33] Miller, P., Freericks, J. K. & Nicol, E. J. Possible experimentally observable effects of vertex corrections in superconductors. *Physical Review B* **58**, 14498 (1998).
- [34] Pietronero, L., Strässler, S. & Grimaldi, C. Nonadiabatic superconductivity. I. vertex corrections for the electron-phonon interactions. *Phys. Rev. B* **52**, 10516–10529 (1995).
- [35] Grimaldi, C., Pietronero, L. & Scattoni, M. The physical origin of the electron-phonon vertex correction. *Eur. Phys. J. B* **10**, 247–255 (1999).
- [36] Grimaldi, C., Pietronero, L. & Strässler, S. Nonadiabatic superconductivity. ii. generalized eliashberg equations beyond Migdal’s theorem. *Phys. Rev. B* **52**, 10530–10546 (1995).
- [37] Pietronero, L. & Strässler, S. Theory of nonadiabatic superconductivity. *Europhys. Lett.* **18**, 627 (1992).
- [38] Giannozzi, P. *et al.* Quantum espresso: a modular and open-source software project for quantum simulations of materials. *J. Phys. Condens. Matter* **21**, 395502 (2009).
- [39] Shamp, A. *et al.* Decomposition products of phosphine under pressure: PH₂ stable and superconducting? *J. Am. Chem. Soc.* **138**, 1884–1892 (2016).
- [40] Sano, W., Koretsune, T., Tadano, T., Akashi, R. & Arita, R. Effect of Van Hove singularities on high- T_C superconductivity in H₃S. *Phys. Rev. B* **93**, 094525 (2016).
- [41] Szczęśniak, R. The numerical solution of the imaginary-axis Eliashberg equations. *Acta Phys. Pol. A* **109**, 179 (2006).
- [42] Szczęśniak, R., Drzazga, E. A. & Szczęśniak, D. Isotropic and anisotropic description of superconducting state in CaC₆ compound. *Eur. Phys. J. B* **88**, 52 (2015).
- [43] Szczęśniak, D. & Szczęśniak, R. Thermodynamics of the hydrogen dominant potassium hydride superconductor at high pressure. *Solid State Commun.* **212**, 1 – 4 (2015).
- [44] Szczęśniak, R., Zemła, T. & Szczęśniak, D. Superconducting state in bromium halide at high pressure. *Physica B* **495**, 106 – 116 (2016).
- [45] Carbotte, J. P. Properties of boson-exchange superconductors. *Rev. Mod. Phys.* **62**, 1027 (1990).
- [46] Marsiglio, F., Schossmann, M. & Carbotte, J. P. Iterative analytic continuation of the electron self-energy to the real axis. *Phys. Rev. B* **37**, 4965–4969 (1988).